

A precessing jet model for the PN K 3-35: simulated radio-continuum emission

Pablo F. Velázquez^{1*}, Yolanda Gómez^{2†}, Alejandro Esquivel^{1‡}, and Alejandro C. Raga^{1§}

¹*Instituto de Ciencias Nucleares, Universidad Nacional Autónoma de México, Ciudad Universitaria,*

Apartado Postal 70-543, CP 04510, México D.F., México.

²*Centro de Radioastronomía y Astrofísica, Universidad Nacional Autónoma de México,*

Apdo. Postal 3-72 (Xangari), CP 58089, Morelia, Michoacán, México.

Accepted . Received ; in original form

ABSTRACT

The bipolar morphology of the planetary nebula (PN) K 3-35 observed in radio-continuum images was modelled with 3D hydrodynamic simulations with the adaptive grid code YGUAZÚ-A. We find that the observed morphology of this PN can be reproduced considering a precessing jet evolving in a dense AGB circumstellar medium, given by a mass loss rate $\dot{M}_{csm} = 5 \times 10^{-5} \text{ M}_{\odot} \text{ yr}^{-1}$ and a terminal velocity $v_w = 10 \text{ km s}^{-1}$. Synthetic thermal radio-continuum maps were generated from numerical results for several frequencies. Comparing the maps and the total fluxes obtained from the simulations with the observational results, we find that a model of precessing dense jets, where each jet injects material into the surrounding CSM at a rate $\dot{M}_j = 2.8 \times 10^{-4} \text{ M}_{\odot} \text{ yr}^{-1}$ (equivalent to a density of $8 \times 10^4 \text{ cm}^{-3}$), a velocity of 1500 km s^{-1} , a precession period of 100 yr, and a semi-aperture precession angle of 20° agrees well with the observations.

Key words: hydrodynamics – methods: numerical – ISM: planetary nebulae: individual K 3-35 – ISM: jets and outflows – radiation mechanisms: thermal

1 INTRODUCTION

The evolution between the end of the asymptotic giant branch (AGB) and the planetary nebula (PN) phases has for a long time been a poorly understood link in the late stages of intermediate-mass stars ($1 - 8 \text{ M}_{\odot}$). It is in this transition phase where the fast stellar wind of the emerging PN interacts with the slow wind from its precursor AGB star (Kwok, Purton, & Fitzgerald 1978), shaping the final morphology of the PN.

Other ingredients that can contribute to the final shape of a PN are the presence of interacting binary stars (e.g. Morris 1987; Balick & Frank 2002; Soker & Bisker 2006) or magnetic fields (e.g. García-Segura & López 2000; Blackman et al. 2001; García-Segura, López & Franco 2005). Thus, the study of objects in this transition phase can give us important clues about the physical mechanisms responsible for the different morphologies observed in PNe.

K 3-35 is a very young PN with a characteristic S-

shaped emission morphology that suggests the presence of precessing bipolar jets (Aaquist & Kwok 1989; Aaquist 1993; Miranda et al. 2000; 2001). The detection of OH and H₂O maser emission as well as the presence of CO and HCO⁺ emission suggest that K 3-35 departed from the proto-PN phase only a few decades ago (Miranda et al. 2001; Tafuya et al. 2007).

Miranda et al. (2001) estimate a dynamical age of ≤ 15 years for the ionised inner core, which expands at $\sim 25 \text{ km s}^{-1}$. For the jets, assuming a modest jet velocity of $\sim 100 \text{ km s}^{-1}$, an age of ~ 800 years is obtained. Therefore, the jet formation in K 3-35 occurred during the proto-PN phase. In this paper we show that the radio morphology of K 3-35 can be explained by a precessing jet model.

2 THE PRECESSING JET MODEL

The PN K 3-35 belongs to the point-symmetric PN group because it shows a bipolar structure, with an ‘S’ shaped morphology in radio-continuum maps at 8.3 GHz (Miranda et al. 2001, 1998; Aaquist 1993; Gómez et al. 2003).

This kind of morphology is more often observed in

* E-mail: pablo@nucleares.unam.mx

† E-mail: y.gomez@astrosmo.unam.mx

‡ E-mail: esquivel@nucleares.unam.mx

§ E-mail: raga@nucleares.unam.mx

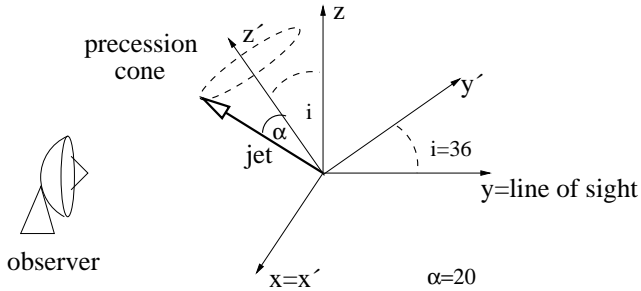


Figure 1. Scheme of the initial conditions for the simulation. The xyz -frame corresponds to the computational domain. The physical system is given by the $x'y'z'$ -frame, which is obtained by rotating the yz -plane around x -axis by 36° with respect to the plane of the sky (xz -plane).

galactic and extragalactic jets. Several theoretical studies have employed precessing jets for modelling these objects and explaining the ‘S’ shape observed at different frequencies.

For instance, in the galactic case, Masciadri et al. (2002) carried out 3D numerical simulations of the HH 34 jets, and compared jet models with and without precession. In the field of extragalactic jets, Rodríguez-Martínez et al. (2006) made a 3D hydrodynamical simulation of a precessing jet moving into an intragalactic cluster medium, and compared their results with the Abell 1795 galaxy cluster. The similarity between these jets and point-symmetric PNe has recently motivated models of this type of PNe as jets, considering precession, density and/or variable ejection velocity, etc., in order to explain their kinematics, emission, and morphology. An excellent review of these works is given by Soker & Bisker (2006).

As an example, we can mention the observational study of the proto-planetary nebula (PPN) Hen 3-1475 by Riera et al. (2003). In $H\alpha$, [NII], and [OIII] images, this PPN exhibits several knots forming an ‘S’ shape. Also Riera et al. (2003) made radial velocity and proper motion studies, showing that the knotty structure of Hen 3-1475 can be explained by means of a jet with a variable ejection velocity and precession. Based on these hypotheses, Velázquez et al. (2004) have computed 2D (axisymmetric) and 3D hydrodynamical simulations of such a jet, showing that this model can reproduce both the observed morphology and the kinematical characteristics of the outflows of Hen 3-1475.

In the present paper, we model the PN K 3-35 with 3D numerical simulations of a precessing jet. Due to the fact that the bipolar structure of K 3-35 looks almost continuous, we do not find necessary to consider also a time variability for the jet velocity and/or density.

In PNe, the surrounding circumstellar medium (CSM) is strongly modified by the central star, which injects material and increases the density of the CSM. Based on the work of Mellema (1995), this perturbed CSM can be described by:

$$\rho(R) = \rho_0 \left[1 - \delta \left(\frac{1 - \exp(-2\beta \sin^2 \theta)}{1 - \exp(-2\beta)} \right) \right] (R_0/R)^2, \quad (1)$$

where $R = \sqrt{x^2 + y^2 + z^2}$ is the distance from the jet source on a 3D Cartesian frame. The angle θ is measured with respect to the equator, which we have chosen to coincide with

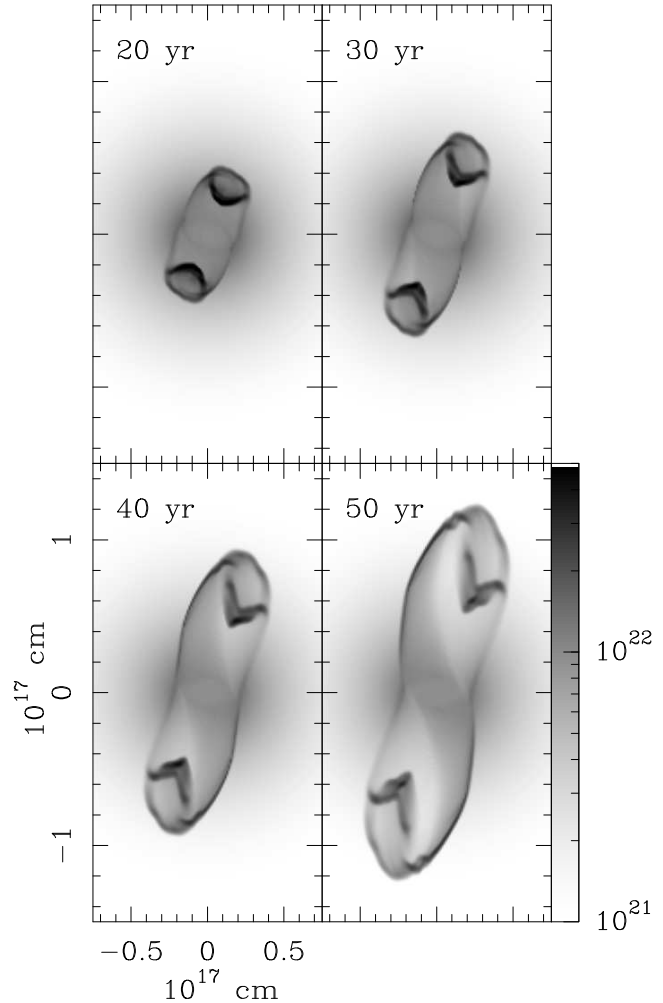


Figure 2. Temporal evolution of the column density at integration times $t = 20, 30, 40, 50$ yrs. These maps were obtained integrating the density along the x -axis. At $t=40$ yr, the jet achieves an extension of 1.8×10^{17} cm, which is equivalent to $2.4''$, i. e., the angular extension of bipolar structure of PN K 3-35 (for an assumed distance of 5 kpc). Both axes are labelled in units of 10^{17} cm, and the bar on the right represents the logarithmic gray-scale, given in units of cm^{-2} .

the xy -plane, yielding $\theta = \tan^{-1}(\sqrt{x^2 + y^2}/z)$. Eq. 1 describes the stratification of the surrounding CSM produced by a star in AGB phase. The parameter δ in Eq. 1 is related to the ratio of the density at the equator (xy -plane) and at the pole (z -axis), and β determines how the density varies from the equator to the pole (Mellema 1995). The value of ρ_0 is calculated from the mass loss rate as : $\rho_0 = \dot{M}/(4\pi R_0^2 v_{\text{env}})$, where v_{env} is the expansion velocity of the AGB remnant.

3 THE NUMERICAL SIMULATIONS

3.1 Initial numerical simulation setup

The numerical simulations were carried out employing the 3D adaptive grid code YGUAZÚ-A (Raga et al. 2000). Together with the gas-dynamic equations, several rate equa-

tions for atomic/ionic species (H I-II, He I-III, C II-IV, and O I-IV) are integrated in order to calculate a non-equilibrium ionisation cooling function for the gas (for temperatures above $\sim 10^5$ K the cooling rate is approximated by an equilibrium ionisation parameterised function). The gas-dynamic equations are integrated with the “flux-vector splitting” algorithm of Van Leer (1982). Details of the reaction and cooling rates included in the code are described in the appendix of Raga et al. (2002) and Raga et al. (2007).

The simulations were performed in a five level, binary adaptive grid, with a maximum resolution of 5.9×10^{14} cm (along the three axes). The computational domain had an extent of 1.5×10^{17} cm in the x - and y -directions, and of 3×10^{17} cm in the z -direction.

Both the cone precession axis and the CSM density distribution were rotated around the x -axis, by 36° with respect to the plane of the sky (yz -plane, see Fig.1). This inclination angle was found by Uscanga et al. (2007), who modelled the H_2O maser emission of the accretion disk around the K 3-35 central star. The configuration is shown in Fig. 1.

The jet is placed at the centre of the computational domain with an initial radius $r_j = 1.5 \times 10^{16}$ cm (equivalent to 30 pixels at the maximum grid resolution) and a length $l_j = 6 \times 10^{15}$ cm. Initially (integration time $t = 0$ yr), the jet axis lying on the $x'z'$ -plane and starts to move (counterclockwise) into a precession cone, with a semi-opening angle $\alpha = 20^\circ$. At $t = 0$ yr, the jet velocity components are $v'_j = (464., 0., 1426.)$ km s $^{-1}$, in the $x'y'z'$ - frame (see fig. 1), or $v_j = (464., -764., 1204.)$ km s $^{-1}$, in the xyz - frame (the computational domain frame). After several tests, a precession period of $\tau_p = 100$ yr was chosen. Two runs were computed considering that the jet material is injected as singly ionised or neutral gas. K 3-35 has a bright centre when it is observed at radiofrequencies, because the central source strongly ionises the CSM gas. This process is not taken into account in our simulations. Since we continuously impose the jet inflow conditions within a cylindrical volume (see §2), when we calculate synthetic radio-continuum maps we obtain a strong central emission component (coming from this cylinder) for the initially ionised jet simulation, giving a good morphological agreement with the observations. However, this central component in the simulated radio emission is exclusively a result of the chosen jet inflow conditions, and for this reason only synthetic maps obtained for the run with the “neutral jet” will be employed for calculating total fluxes.

A good fit with the observations is obtained when the velocity and mass loss rate of the jet were set to 1,500 km s $^{-1}$ and $\dot{M}_j = 2.8 \times 10^{-4} M_\odot$ yr $^{-1}$, respectively. These parameters let an equivalent density ρ_j of 8×10^4 cm $^{-3}$. The neutral CSM is modelled by Eq.1, with a mass lose rate $\dot{M} = 5 \times 10^{-5} M_\odot$ yr $^{-1}$, $v_w = 10^6$ cm s $^{-1}$, and the parameters δ and β , were set to 0.1 and 3, respectively. These parameters give an almost isotropic density distribution with a contrast of 20% between the density at the equator and the poles. From this relationship, densities between 7.5×10^{-19} g cm $^{-3}$ and 1.7×10^{-20} g cm $^{-3}$ are obtained for distances from the source of 1.5×10^{16} cm and 10^{17} cm along the z' - direction, respectively. These high densities are supported by the recent detection of HCO^+ toward K 3-35, that reveals the presence of high density molecular gas (Tafuya et al. 2007).

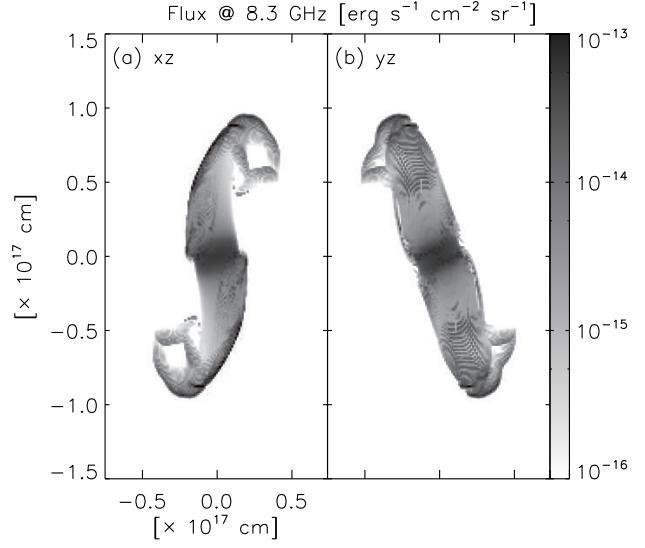


Figure 3. Simulated thermal radio-continuum maps obtained for a frequency of 8.3 GHz. The left panel is the emission map generated by integrating the emission coefficient along the y -axis, the right panel is the result of integrating along the x -axis. The bar on the right shows the logarithm gray-scale of the radio thermal emission in units of $\text{erg s}^{-1} \text{cm}^{-2} \text{sr}^{-1}$. Both spatial axis are in units of 10^{17} cm. Strong emission is observed in the centre due to the fact that this is the region where a singly ionised jet inflow condition is continuously imposed.

Taking into account the CSM density distribution, and the jet density and velocity, it is possible to estimate the speed of the leading ‘working surface’ (i. e. the head) of the jet :

$$v_{ws} = v_j \frac{\sqrt{\rho_j / \rho_{csm}(R, \theta)}}{\sqrt{\rho_j / \rho_{csm}(R, \theta)} + 1}, \quad (2)$$

where v_j is the jet injection velocity, and ρ_j and ρ_{csm} are the jet and CSM densities, respectively. It is straightforward to show from Eqs. (2) and (1) that for large distances R from the jet source, v_{ws} increases. For instance, considering the values for v_j , ρ_j , and ρ_{csm} , speeds of 4.4×10^2 km s $^{-1}$ and 1.1×10^3 km s $^{-1}$, are found at $R = 5 \times 10^{16}$ cm and $R = 10^{17}$ cm, respectively.

3.2 Calculation of the thermal radio-continuum emission

To generate synthetic thermal radio-continuum maps, the radiative transfer equation was integrated along different lines of sight.

First, the optical depth $\tau_\nu(l)$ was calculated by integrating the absorption coefficient κ_ν along lines of sight : $\tau_\nu(l) = \int_0^l \kappa_\nu dl$ (with l being the spatial coordinate along the line of sight). The absorption coefficient κ_ν is given by (Rybicki & Lightman 1979; Osterbrock 1989):

$$\kappa_\nu = 0.018 T^{-3/2} n_e n_i \nu^{-2} g_{ff}, \quad (3)$$

where $g_{ff} = 0.5513 (\ln(T^{3/2} \nu^{-1}) + 17.7)$ is the Gaunt factor. We obtain directly from our simulations T , n_e , and n_i (the spatial distributions of temperature, electronic, and ionic

| ν (GHz) | S_{40}^{sim} (mJy) | S_{50}^{sim} (mJy) | S_{obs} (mJy) |
|-------------|----------------------|----------------------|-----------------|
| 1.5 | 21.7 | 13.4 | 11.8 to 18.4 |
| 2.4 | 20.6 | 15.5 | — |
| 5.0 | 20.0 | 18.6 | 22.0 ± 2.2 |
| 8.3 | 17.8 | 19.9 | — |
| 10.0 | 17.4 | 20.0 | — |
| 15.0 | 16.4 | 19.8 | 24.0 ± 2.4 |
| 22.0 | 15.5 | 19.1 | 22.0 ± 2.2 |

Table 1. Total flux densities (in units of mJy) at different frequencies, obtained from the simulated images at $t = 40$ yr (second column), and at $t = 50$ yr (third column). In this calculation, a distance of 5 kpc has been assumed to PN K 3-35. These flux densities have been obtained from the simulation where the jet material is imposed as neutral gas, in order to avoid an unrealistic strong emission from the centre. For a direct comparison with observations, the fourth column gives the “halo” observed fluxes, taken from Aaquist (1993).

number densities, respectively), which are used in Eq. (3) to calculate κ_ν (in units of cm^{-1}).

Then, the intensity as a function of frequency can be obtained as :

$$I_\nu = \int_0^l j_\nu(n_e, n_i, T) e^{-\tau_\nu(l)} dl, \quad (4)$$

where j_ν is the emission coefficient (which is a function of T , n_e , and n_i). The intensity I_ν has units of $\text{erg s}^{-1} \text{sr}^{-1} \text{cm}^{-2} \text{Hz}^{-1}$. Numerically, the emission coefficient can be calculated using the following equation (Rybicki & Lightman 1979; Osterbrock 1989):

$$j_\nu = 5.4113 \times 10^{-39} n_e n_i T^{-1/2} e^{-h\nu/kT} g_{\text{ff}}, \quad (5)$$

where h and k are the Planck’s and Boltzmann’s constants, respectively. The coefficient j_ν has units of $\text{erg s}^{-1} \text{sr}^{-1} \text{cm}^{-3} \text{Hz}^{-1}$.

Synthetic maps at different frequencies were generated combining the results from the 3D simulation with Eqs. (3), (4), and (5). The angularly integrated fluxes (in mJy) corresponding to different frequencies were then determined from the simulated maps, assuming a distance to the source of 5 kpc (Zhang 1995).

4 RESULTS

With the physical conditions described in §3.1, a 3D numerical simulation was carried out. Figure 2 shows the temporal evolution of the column density obtained for integration times lying in the range [20,50] yrs. The stratification of the surrounding CSM is clearly observed in all maps.

Filamentary structures are observed at the head jets, due to precession movement. At different times, jet material is injected at different angles. These jet material sweep up the CSM which have a density stratification as function of the angle (see Eq. 1), generating the bright filaments observed in the column density maps.

At a $t = 40$ yr integration time, the jet reaches a total length of 1.8×10^{17} cm. This size is equivalent to $2.4''$ (i. e., the angular extension of K 3-35 on the plane of the sky), at a distance of 5 kpc. Miranda et al. (2001) have made estimates

of the dynamical ages of both the inner ionised core and the extended emission (jets) of the PN K 3-35. Based on an expansion rate of $\sim 25 \text{ km s}^{-1}$ taken from the He II lines, they obtained a dynamical age of ≤ 15 yr for the core, while assuming a jet velocity of $\sim 100 \text{ km s}^{-1}$, a dynamical age of ~ 800 yr is deduced for the jets. Our simulations required a much larger jet velocity to explain the radio emission of the lobes in the PN K 3-35, thus yielding a short dynamical age for the jets, which is comparable with that of the core. This is interesting because it may suggests that the process that originated the ionisation of the jets and the core occurred almost simultaneously.

Synthetic maps were generated (as described in section 3.2) for the following frequencies: 1.5, 2.4, 5, 8.3, 10, 15, and 22 GHz. Very similar morphologies are obtained for all of these frequencies. Figure 3 shows the maps obtained at 8.3 GHz. The left panel of Figure 3 displays the simulated radio-continuum emission when the $j_{8.3\text{GHz}}$ (Eq. 5) is integrated along the y -axis, giving the emission on the xz -plane. The right panel of Figure 3 shows the 8.3 GHz emission on the yz -plane (i. e., the integration of $j_{8.3\text{GHz}}$ was carried out along the x -axis). The map on the right was shown to illustrate how the morphology strongly depends on the projection chosen. In the xz -projection, the radio emission has an ‘S’ shape (which is the morphology of K 3-35), while in the yz -projection, we have a ‘Z’ shape. These maps are displayed in units of $\text{erg cm}^{-2} \text{s}^{-1} \text{sr}^{-1}$.

Comparing the left panel of Figure 3 with the column density map at $t = 40$ yr of Figure 2, we see that the radio-continuum emission traces very well the precessing jet morphology.

It is also possible to compare simulated and observed total fluxes. However, since we are not simulating the radio emission from the central region, we can only compare the radio emission from the lobes or jets, which were called the ‘halo’ in Aaquist (1993). From each simulated radio map we measured the corresponding total flux from these structures. These fluxes are listed in Table 4, where one can see that the total fluxes in the simulations (at all frequencies) are of the order of the observed ones. At an integration time of 40 yr, the simulated flux gives an optically thin behaviour for the spectrum. On the other hand, for integration times of 50 yr, the simulated flux has a maximum at a frequency between 5 and 8.3 GHz, in good agreement with the Aaquist (1993) results. At frequencies higher than 8.3 GHz, the spectral index is of -0.09 , which corresponds to optically-thin thermal free-free emission.

A direct comparison between both observed and simulated 8.3 GHz maps is shown in Figure 4. The simulated map was convolved with a synthesised beam of $0.2'' \times 0.2''$ (similar to the beam in the observations), and scaled to yield units of mJy beam^{-1} . The same scale for both images have been employed. Also, the synthetic map was tilted in 48° (with respect to z - axis, see Fig. 1) in order to do the position angle (P.A) of the jet direction (in the xz - plane) equal to 65° , the observed P.A.(Miranda et al. 2001).

5 SUMMARY

Several 3D hydrodynamical simulations were carried out employing the adaptive grid code YGUAZÚ-A, in order to model

both the morphology and the thermal radio emission of the planetary nebula K 3-35.

After analysing our results, we found that the bipolar structure of this PN can be described as the result of the interaction of a dense jet (with an initial number density of $8 \sim 10^4 \text{ cm}^{-3}$ or $\dot{M}_j = 2.8 \times 10^{-4} M_\odot \text{ yr}^{-1}$) moving into a dense environment, previously swept up by the AGB wind of the central star.

The ‘S’ morphology shown by K 3-35 in 8.3 GHz radio-continuum images (Miranda et al. 1998, 2001; Gómez et al. 2003) can be reproduced if the modelled jet precesses with a period of 100 yrs on a cone with a half-opening angle of 20° .

For an integration time of 40 yrs, the simulated jet has a total length of $1.8 \times 10^{17} \text{ cm}$, which is equivalent to $2.4''$ (Miranda et al. 2001; Gómez et al. 2003) considering an estimated distance of 5 kpc to K 3-35 and also the orientation of this object (Uscanga et al. 2007). This time is almost 20 times smaller than the one given by Miranda et al. (2001) for the jet, where a slower velocity was assumed. However, it is only 2.7 times larger than the dynamical age of the inner core (also in Miranda et al. 2001), suggesting that the two events are more related than previously thought, and further supporting the idea that K 3-35 is a young object.

Synthetic radio-continuum maps were generated from our numerical results. These maps show that the predicted morphologies and fluxes are in reasonable agreement with the observations. At an integration time of 40 yrs, the obtained spectral index is the one of optically thin emission. For an integration time of 50 yrs, the observed change of the spectral index with frequency (Aaquist 1993) is also reproduced by our simulation. A direct comparison between the observational and numerical results is given in Fig. 4, where we show the observed and synthetic (for an integration time of 40 yrs) 8.3 GHz radio maps.

We must note that the values for the velocity and mass loss rate employed in the simulation for the jet and the CSM seem to be rather high. It is difficult for AGB and post-AGB stars to launch jets at velocities of the order of 1500 km s^{-1} (although Riera et al. 2003 have reported this kind of velocity for the outflows of the PPN 3-1475). Besides, the mass injection is also a bit extreme, in 40 years both jets have injected $0.02 M_\odot$ into the surrounding CSM. This scenario might be explained in terms of a binary system, if the jet is produced by a companion accreting material (at a rate about ten times higher than \dot{M}_j) from a massive star (the AGB progenitor that produced the density distribution of the circumstellar material). The primary in the last 40 years has lost $0.2 M_\odot$. This means that it started with an envelope containing this mass, which appears to correspond to an AGB star rather than a post-AGB star (even though at the present time the star has already evolved to the planetary nebula stage).

Furthermore, the CSM is very dense. With the parameters employed, in a radius of 10^{17} cm , a mass of $1 M_\odot$ is contained, implying a massive PN. There is observational evidence that favours a very dense surrounding CSM. However, the total mass derived from HCO^+ observations (Tafaya et al. 2007) is quite low ($\sim 0.017 M_\odot$), so that the molecular emission from this molecule would be confined to a small, possibly shock excited volume, in order to be consistent with our much higher mass CSM. These values imply

that this scenario would be plausible if it is a short lived event. Clearly, a better determination of these parameters could be done with proper motion studies and better distance determinations.

Notwithstanding the extreme values for the employed parameters, it is important to note that a simple model of a precessing dense jet moving into an also dense CSM, successfully reproduces the observed morphology of the PN K 3-35, obtaining a qualitatively and quantitatively good agreement between the model predictions and the observations, although this scenario would be a short lived event.

ACKNOWLEDGEMENTS

The authors acknowledge support from CONACyT grant 46628-F, and DGAPA-UNAM grants IN108207 and IN100407. The work of ACR, AE, and PFV was supported by the “Macroproyecto de Tecnologías para la Universidad de la Información y la Computación” (Secretaría de Desarrollo Institucional de la UNAM, Programa Transdisciplinario en Investigación y Desarrollo para Facultades y Escuelas, Unidad de Apoyo a la Investigación en Facultades y Escuelas). Authors sincerely acknowledge Noan Soker (the referee) for his very useful comments, which allow us to improve the previous version of this manuscript. We also would like to thank the computational team of ICN: Antonio Ramírez and Enrique Palacios, for maintaining and supporting our Linux servers, and Martín Cruz for the assistance provided. Finally, PFV acknowledges the hospitality, during his visits, of the CRyA (campus Morelia-UNAM) staff.

REFERENCES

- Aaquist, O. B. 1993, *A&A*, 267, 260
- Aaquist, O. B. & Kwok, S. 1989, *A&A*, 222, 227
- Balick, B., & Frank, A. 2002, *ARA&A*, 40, 439
- Blackman, E. G., Frank, A., Markiel, J. A., Thomas, J. H., & Van Horn, H. M. 2001, *Nature*, 409, 485
- García-Segura, G., & López, J. A. 2000, *ApJ*, 544, 336
- García-Segura, G., López, J. A., & Franco, J. 2005, *ApJ*, 618, 919
- Gómez, Y., Miranda, L. F., Anglada, G., & Torrelles, J. M. 2003, *Planetary Nebulae: Their Evolution and Role in the Universe*, 209, 263
- Kwok, S., Purton, C. R., & Fitzgerald, P. M. 1978, *ApJ*, 219, L125
- Masciadri, E., de Gouveia Dal Pino, E. M., Raga, A. C., & Noriega-Crespo, A. 2002, *ApJ*, 580, 950
- Mellema, G. 1995, *MNRAS*, 277, 173
- Miranda, L. F., et al. 2000, *MNRAS*, 311, 748
- Miranda, L. F., Torrelles, J. M., Guerrero, M. A., Aaquist, O. B., & Eiroa, C. 1998, *MNRAS*, 298, 243
- Miranda, L. F., Gómez, Y., Anglada, G., & Torrelles, J. M. 2001, *Nature*, 414, 284
- Morris, M. 1987, *PASP*, 99, 1115
- Osterbrock, D. E. 1989, Research supported by the University of California, John Simon Guggenheim Memorial Foundation, University of Minnesota, et al. Mill Valley, CA, University Science Books, pp. 86-96.

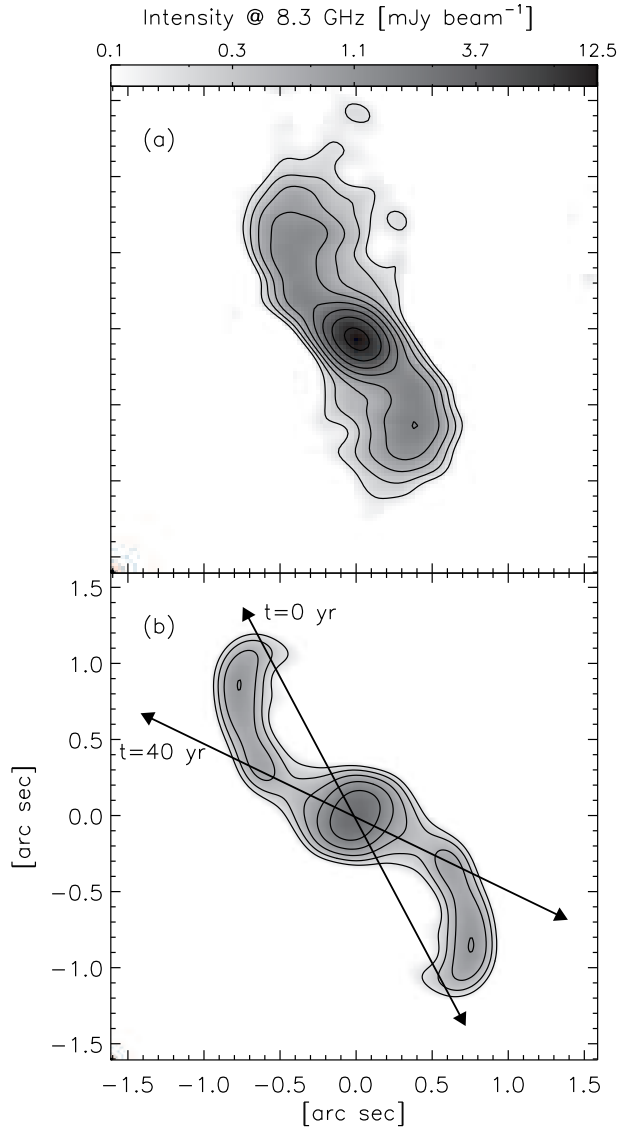


Figure 4. Comparison between observational and numerical results. The top panel shows the 8.3 GHz radio continuum image of K 3-35 (Miranda et al. 2001; Gómez et al. 2003). The bottom panel shows the tilted synthetic radio emission map at the same frequency, obtained for an integration time of 40 yr. An inclination of 36° between the precession axis and the plane of the sky was considered. The simulated map was smoothed with the observed beam of $0.2'' \times 0.2''$ and it is shown in the same scale that the observed one. The contours corresponds to the levels 0.18, 0.31, 0.56, 1.0, 1.78, 3.16, 5.62, and 10.00 mJy beam⁻¹. The arrows indicate the jet direction (projected on the plane of the sky) for integrations times of 0 and 40 yr. The last one is coincident with the P.A. measured by Miranda et al. (2001).

- Riera, A., García-Lario, P., Manchado, A., Bobrowsky, M., & Estalella, R. 2003, *A&A*, 401, 1039
 Rodríguez-Martínez, M., Velázquez, P. F., Binette, L., & Raga, A. C. 2006, *A&A*, 448, 15
 Rybicki, G. B., & Lightman, A. P. 1979, in *Radiative Processes in Astrophysics*, New York, Wiley-Interscience, pp. 159-163.
 Soker, N., & Bisker, G. 2006, *MNRAS*, 369, 1115
 Tafoya, D., et al. 2007, *AJ*, 133, 364
 Uscanga, L. et al, 2007, in preparation.
 Van Leer, B., ICASE Report No. 82-30.
 Velázquez, P. F., Riera, A., & Raga, A. C. 2004, *A&A*, 419, 991
 Zhang, C. Y. 1995, *ApJS*, 98, 659

This paper has been typeset from a \LaTeX file prepared by the author.

- Raga, A. C., Navarro-González, R., & Villagrán-Muniz, M. 2000, *Revista Mexicana de Astronomía y Astrofísica*, 36, 67
 Raga, A. C., de Gouveia Dal Pino, E. M., Noriega-Crespo, A., Mininni, P. D., & Velázquez, P. F. 2002, *A&A*, 392, 267
 Raga, A. C., De Colle, F., Kajdič, P., Esquivel, A., Cantó, J. 2007, *A&A*, 465, 879